Chinese Chemical Letters 37 (2026) 112607

Contents lists available at ScienceDirect

Chinese Chemical Letters

journal homepage: www.elsevier.com/locate/cclet

Ultrafast microwave *quasi*-solid-synthesized Ru-loaded tungsten-molybdenum phosphide with coral-like architectures for electrocatalytic hydrogen generation

Xueying Luan[a,1], Huilin Zhao[a,1], Yuhao Li[a], Yusen Chen[a], Hongdong Li[a], Jun Xing[a], Yingxia Zong[a], Weiping Xiao[b], Guangying Fu[c], Jinsong Wang[d], Lei Wang[a,*], Zexing Wu[a,*]

[a] *Key Laboratory of Eco-chemical Engineering, Ministry of Education, International Science and Technology Cooperation Base of Eco-chemical Engineering and Green Manufacturing, College of Chemistry and Molecular Engineering, Qingdao University of Science & Technology, Qingdao 266042, China*
[b] *College of Science, Nanjing Forestry University, Nanjing 210037, China*
[c] *Key Laboratory of Photoelectric Conversion and Utilization of Solar Energy, Qingdao Institute of Bioenergy and Bioprocess Technology, Chinese Academy of Sciences, Qingdao 266101, China*
[d] *Faculty of Materials Science and Engineering, Kunming University of Science and Technology, Kunming 650093, China*

ARTICLE INFO

Article history:
Received 25 December 2025
Revised 25 February 2026
Accepted 9 March 2026
Available online 10 March 2026

Keywords:
Electrocatalyst
Tungsten-molybdenum phosphide
Hydrogen evolution reaction
Electronic metal-support interaction
Microwave

ABSTRACT

Electronic metal-support interaction (EMSI) offers a revolutionary strategy for designing high-performance electrocatalysts by precisely modulating interfacial electron transfer dynamics. Herein, we construct a Ru-loaded tungsten-molybdenum bimetallic phosphide heterostructure (Ru/WP-MoP) through EMSI engineering, which demonstrates exceptional hydrogen evolution reaction (HER) performance across pH-universal electrolytes. The optimized catalyst presents a remarkably low overpotential of 40 mV at 10 mA/cm^2 in alkaline media, outperforming Ru/C ($\eta_{10} = 52$ mV). Remarkably, it retains significant activity even under acidic conditions ($\eta_{10} = 55$ mV) and alkaline seawater ($\eta_{10} = 42$ mV). In alkaline media, it operates continuously at 200 mA/cm^2 for 55 h with current density decay of less than 2 %. Combined X-ray photoelectron spectroscopy analysis reveals that the strong EMSI effect induces electron transfer from WP-MoP to Ru, optimizing the d-band center position and reducing the water dissociation energy barrier compared with monometallic counterparts. This work establishes a general paradigm for developing robust transition metal phosphide catalysts *via* interfacial electronic structure manipulation, particularly for industrial-scale seawater electrolysis applications.

© 2026 Published by Elsevier B.V. on behalf of Chinese Chemical Society and Institute of Materia Medica, Chinese Academy of Medical Sciences.

The excessive consumption of fossil fuels causes severe environmental degradation and remains a dominant contributor to global climate change [1–3]. The critical situation necessitates accelerating the development of renewable energy alternatives, with hydrogen energy standing out as a strategically vital solution. Recognized for its carbon-neutral combustion characteristics and scalable production potential, hydrogen is positioned to play a pivotal role in future energy systems [4–6]. Water electrolysis, as a zero-emission hydrogen production technology, demonstrates particular promise for displacing conventional carbon-intensive energy carriers [7,8]. As the cathodic reaction in water-splitting, the hydrogen evolution reaction (HER) requires advanced electrocatalysts that determine overall energy conversion efficiency [9]. Although platinum-based catalysts currently remain the benchmark for HER activity, their exorbitant cost underscores the urgent need to develop synthesis protocols enabling rapid fabrication of Ru-based catalysts with high intrinsic activity ($\eta_{10} < 50$ mV) and long-term stability [10].

Transition metal phosphides (TMPs) exhibit immense potential in electrocatalysis due to their high electrical conductivity and unique crystal structures [11]. Specifically, phosphorus (P) atoms with higher electronegativity are embedded within the prismatic frameworks of TMPs, acting as proton adsorption centers that significantly enhance electrocatalytic activity through multielement synergistic effects [12,13]. These advantages position TMPs as efficient multifunctional catalysts in energy storage technologies and clean fuel production [14]. However, their practical applications are challenged by mismatch between the electrocatalytic performance and real-world demands. Strategies, such as morphology regulation and element-doping-induced synergistic effects of electronic metal-support interaction (EMSI), are of profound

* Corresponding authors.
E-mail addresses: inorchemwl@126.com (L. Wang), splswzx@qust.edu.cn (Z. Wu).
[1] The authors contribute equally to this work.

https://doi.org/10.1016/j.cclet.2026.112607
1001-8417/© 2026 Published by Elsevier B.V. on behalf of Chinese Chemical Society and Institute of Materia Medica, Chinese Academy of Medical Sciences.

significance for boosting electrocatalytic performance [15–17]. For instance, element doping not only elevates the density of active sites but also enhances water dissociation kinetics by modifying coordination configurations [18]. For example, Dong *et al.* prepared a W-doped NiCo phosphide, in which W, Ni, and Co ternary metals are electrodeposited and anchored on nickel foam. The W sites can efficiently convert H* to H_2, and the overpotential of W-NiCoP/NF at 10 mA/cm^2 is 29.6 mV for HER [19]. However, the synthesis strategies for tungsten-molybdenum-based metal phosphides differ distinctly from those for general transition metal phosphide catalysts. Existing strategies mainly consist of two high-temperature strategies: Inert gas-assisted phosphorization of precursors at 750 °C and hydrogen-assisted reduction of tungstate-molybdate at 800 °C [20,21]. However, these routes suffer from high energy consumption, prolonged processing duration, and safety hazards posed by PH_3 byproducts. There is thus an urgent need to develop scalable, eco-friendly strategies for the fabrication of tungsten-molybdenum-based metal phosphides.

In this study, an efficient and scalable ultrafast microwave-assisted *quasi*-solid-state strategy is developed to introduce W, Mo, Ru ternary metals to induce EMSI interactions for the preparation of highly catalytic Ru/WP-MoP catalysts. The ternary synergy effectively modulates the electronic structure and enhances the HER performance: The catalyst achieves 10 mA/cm^2 current density with 40/42/55 mV overpotentials in 1 mol/L KOH, 1 mol/L KOH-containing seawater, and 0.5 mol/L H_2SO_4, respectively, outperforming Ru/C, and has excellent stability. In overall water splitting, 10 mA/cm^2 current density is achieved at 1.44 V, demonstrating excellent catalytic ability. This work realizes the low-temperature rapid fabrication of transition metal phosphides and proposes a new path for the construction of advanced electrocatalytic materials by regulating atomic coordination through a multi-element strategy.

The Ru/WP-MoP catalyst was synthesized *via* a microwave *quasi*-solid-state strategy, where sodium tungstate hexahydrate, sodium molybdate, and ruthenium trichloride precursors undergo 20 s reaction (Fig. 1a). X-ray diffraction (XRD) analysis (Fig. 1b and Fig. S1 in Supporting information) reveals distinct diffraction patterns matching WP (PDF#29-1364), MoP (PDF#24-0771), and metallic Ru (PDF#06-0663). This demonstrates the successful preparation of WP, MoP, WP-MoP and Ru/WP-MoP. Scanning electron microscopy (SEM) images (Figs. 1c and d) demonstrate the coral-like 3D architecture with hierarchical porosity, where Ru incorporation (Fig. S2 in Supporting information) maintains the WP-MoP framework without morphological changes. High-resolution transmission electron microscope (HR-TEM) analysis (Fig. 1e) resolves lattice spacings of 0.209 nm (MoP (101)), 0.203 nm (WP (211)), consistent with XRD-indexed planes [22–24]. Low–magnification TEM (Fig. 1f) further illustrates the overall coral–like and porous morphology of the Ru/WP–MoP catalyst. Energy dispersive X-ray spectroscopy (EDS) analysis (Fig. 1g) additionally verifies the uniform distribution of W, Ru, Mo, and P.

The electronic structure and chemical states of the elements were further explored *via* X-ray photoelectron spectroscopy (XPS). The successful loading of Ru onto the WP-MoP carrier is confirmed by the XPS survey spectrum (Fig. 2a). Analysis of the W 4f orbitals in both WP-MoP and Ru/WP-MoP reveals three distinct peaks upon deconvolution (Fig. 2b). The peaks at 31.3/33.4 eV and 32.0/34.1 eV are characteristic of W and W^{4+} species, respectively, while the peaks at 36.1/38.3 eV correspond to W^{6+} [25,26]. A comparison of the W 4f spectra between WP-MoP and Ru/WP-MoP shows that the binding energy of the latter is higher, indicating that Ru addition modulates the W atomic configuration and facilitates electron transfer from W to Ru. The Mo 3d peaks in Ru/WP-MoP can be deconvoluted into two sets of peaks at 228/231 eV and 233/236 eV, assigned to the Mo^{4+} and Mo^{6+} oxidation states, respectively

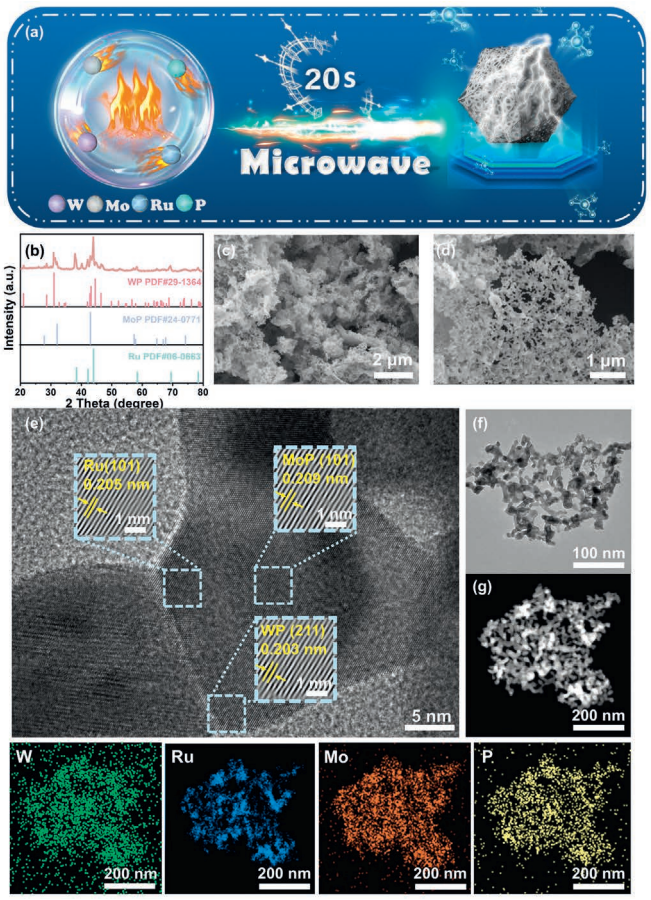


Fig. 1. (a) Schematic illustration of the synthesis route for Ru/WP-MoP. (b) XRD pattern of Ru/WP-MoP. SEM images of (c) WP-MoP and (d) Ru/WP-MoP. (e) High- and (f) low-resolution TEM images of Ru/WP-MoP. (g) S-TEM image with EDS mappings of W, Ru, Mo and P.

(Fig. 2c) [27,28]. Interestingly, the Mo 3d peaks shift positively upon Ru incorporation, further confirming the electron transfer between Mo and Ru. The P 2p peaks at 129.4/130.4 eV (P $2p_{3/2}$ and P $2p_{1/2}$) and an additional peak at 134 eV is assigned to surface-oxidized P (Fig. 2d) [29,30]. In Ru 3p spectrum (Fig. 2e), the presence of Ru^0 and Ru^{4+} species results from the strong electronic interactions between W, Mo, and Ru [31,32]. Additionally, the formation of P vacancies serves as an efficient approach for regulating the electronic structure of the catalyst [33–35]. Electron paramagnetic resonance (EPR) spectra of WP, MoP, WP-MoP, and Ru/WP-MoP (Fig. 2f) reveal a stronger peak at $g = 2.003$ for Ru/WP-MoP and other samples, confirming the creation of P vacancies in the catalyst [36]. The generation of vacancies is conducive to activating the EMSI effect between metal ions, which further improves the HER performance.

A systematic evaluation of the electrocatalytic properties for Ru/WP-MoP and comparative catalysts was conducted in 1 mol/L KOH. As depicted in the linear sweep voltammetry (LSV) curves (Fig. 3a), Ru/WP-MoP demonstrates superior catalytic activity compared with the benchmarked Ru/C (52 mV) and other control samples (WP-MoP, MoP, and WP), achieving 10 mA/cm^2 with a low overpotential of 40 mV. Kinetic analysis through Tafel slopes further confirms the enhanced reaction kinetics of Ru/WP-MoP, displaying a notably smaller slope of 50 mV/dec relative to other counterparts (53-143 mV/dec), indicating its optimized reaction kinetics (Fig. 3b) [12]. Thus, the integration of bimetallic phosphides, Ru incorporation and P vacancies play key role in promoting the electrocatalytic performance. Electrochemical characterization re-

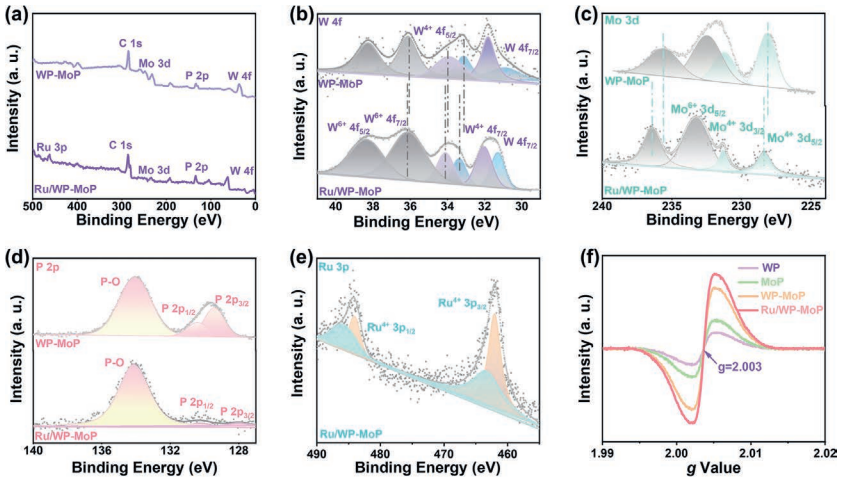


Fig. 2. (a) XPS survey spectra of WP-MoP and Ru/WP-MoP. XPS spectra of (b) W 4f, (c) Mo 3d, and (d) P 2p in WP-MoP and Ru/WP-MoP. (e) Ru 3p spectrum in Ru/WP-MoP. (f) EPR spectra of WP, MoP, WP-MoP and Ru/WP-MoP.

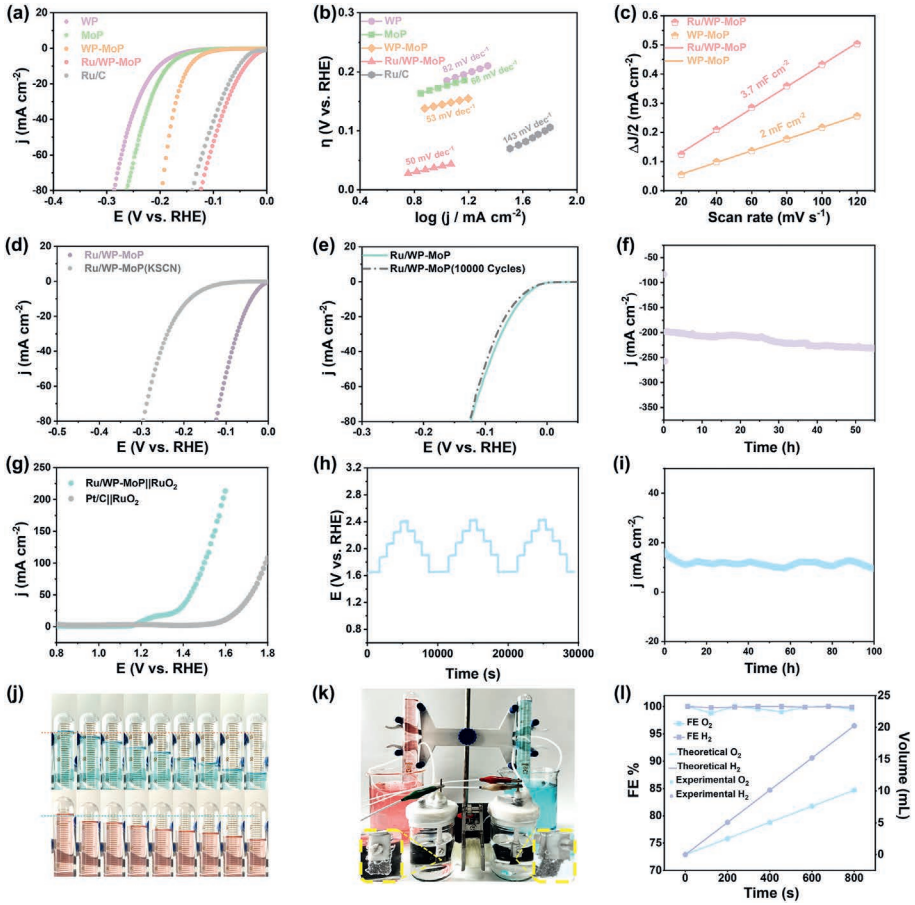


Fig. 3. (a) The LSV curves of WP, MoP, WP-MoP, Ru/WP-MoP and Ru/C in 1 mol/L KOH. (b) Tafel plots. (c) C_{dl} plots. (d) Poisoning experiments. (e) LSV curves before and after 10,000 CV cycles. (f) *I-t* test of Ru/WP-MoP. (g) The overall water splitting (OWS) curves, (h) multi-step chronopotentiometry and (i) stability test of Ru/WP-MoP/NiFe||RuO_2/NiFe in a 1 mol/L KOH solution. (j) Measurement of hydrogen and oxygen production by bubble drainage method. (k) Photographs of hydrogen and oxygen collected at different time. (l) Faraday efficiency diagram.

veals that Ru/WP-MoP possesses 2.3-fold larger electrochemically active surface area (ECSA) than that of WP-MoP (Fig. 3c and Fig. S3 in Supporting information), confirming the critical role of Ru in creating additional active sites. Mechanistic insight is provided by a potassium thiocyanate (KSCN) poisoning experiments, which show a 78.5 % decrease in activity after thiocyanate adsorption (Fig. 3d), indicating Ru serves as the dominant active center [37,38]. Stability evaluations show that the overpotential decay is negligible after 10,000 CV cycles, verifying its excellent durability (Fig. 3e). And the catalyst maintains stable operation for 55 h at 200 mA/cm^2 (Fig. 3f). Evidently, the electrocatalytic performance surpasses that of most reported Ru-based catalysts (Fig. S4 and Table S1 in Supporting information).

Seawater, as a renewable resource, holds significant potential for hydrogen production. Ru/WP-MoP demonstrates exceptional hydrogen evolution capability in alkaline seawater, with an over-

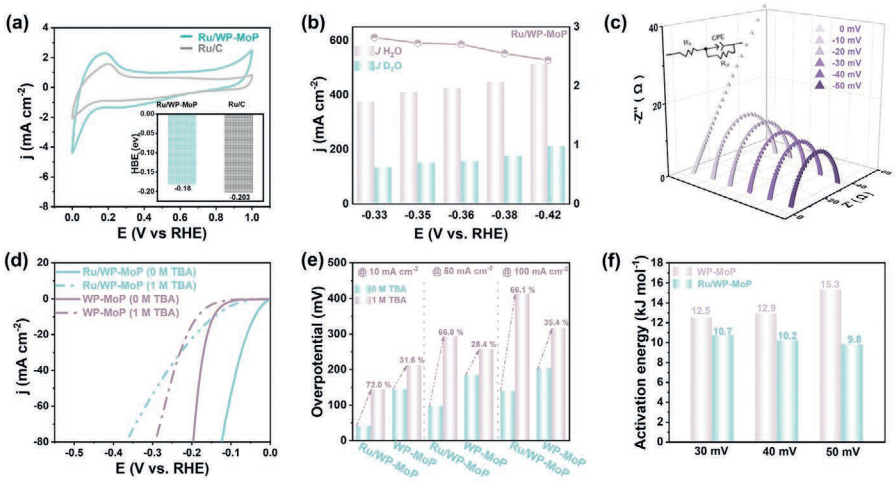


Fig. 4. (a) CV curves of Ru/WP-MoP and Ru/C catalysts in Ar-saturated 1 mol/L KOH. (b) KIE values of Ru/WP-MoP under the corresponding potentials. (c) Nyquist plots for Ru/WP-MoP catalyst at various overpotentials. (d) LSV curves of Ru/WP-MoP in 1 mol/L TBA. (e) Overpotentials of Ru/WP-MoP and WP-MoP with and without 1 mol/L TBA. (f) Activation energies of Ru/WP-MoP and WP-MoP at various overpotentials.

potential of 42 mV at 10 mA/cm^2, significantly lower than control catalysts (WP: 317 mV, MoP: 381 mV, WP-MoP: 224 mV, Fig. S5a in Supporting information). Furthermore, Ru/WP-MoP exhibits favorable reaction kinetics, as evidenced by its smaller Tafel slope (73 mV/dec *vs*. 89-113 mV/dec for counterparts, Fig. S5b in Supporting information). The ECSA, reflected by the double-layer capacitance (C_{dl}), is 5.1 times larger for Ru/WP-MoP (2.85 mF/cm^2) than for WP-MoP (0.56 mF/cm^2), confirming that Ru creates abundant active sites through defect engineering (Figs. S5c and S6 in Supporting information). To identify the catalytic active sites, KSCN poisoning experiment was conducted. The catalytic performance of Ru/WP-MoP decreases by 83 % after poisoning, directly confirming the critical role of Ru active sites for HER (Fig. S5d in Supporting information). Electrochemical impedance spectroscopy (EIS, Fig. S5e in Supporting information) indicates that Ru/WP-MoP possesses the lowest charge transfer resistance (R_{ct}), indicating favorable charge transport dynamics. Regarding stability, the catalyst maintains steadily without significant degradation over 27 h (Fig. S5f in Supporting information). In comparison to other Ru-based catalysts, its catalytic activity remains more efficient than leading seawater HER catalysts reported in the literature. (Fig. S5g and Table S2 in Supporting information).

Ru/WP-MoP also demonstrates exceptional catalytic activity in acidic media (0.5 mol/L H_2SO_4), requiring only 55 mV at 10 mA/cm^2, far smaller than the values obtained for Ru/C (95 mV) and control metal phosphides (141-198 mV, Fig. S7a in Supporting information). Kinetic analysis reveals its Tafel slope of 53 mV/dec, which outperforms all counterparts (57-94 mV/dec), indicating superior reaction kinetics (Fig. S7b in Supporting information). The C_{dl} (Figs. S7c-e in Supporting information) shows that Ru/WP-MoP features an enhanced electrochemically active surface area, implying increased available active sites. This feature can be attributed to the hierarchical porous architecture of Ru/WP-MoP and the high dispersion of Ru species. In the H_2SO_4/D_2O system, the KIE value is 2.5, which further confirms that proton transfer is involved in the rate-determining step for HER (Figs. S7f and g in Supporting information) [39], while KSCN poisoning experiments validate Ru centers as primary active sites (78.5 % activity loss, Fig. S7h in Supporting information). The catalyst operates at 10 mA/cm^2 for 22 h, illustrating its excellent stability (Fig. S7i in Supporting information).

The outstanding HER activity of the Ru/WP-MoP catalyst prompts a systematic evaluation of its practical feasibility. An alkaline electrolysis cell is constructed using Ru/WP-MoP||NiFe as the cathode and benchmark RuO_2||NiFe as the anode. As evidenced in Fig. 3g, the cell achieves only 1.44 V at 10 mA/cm^2, significantly superior to that of the RuO_2||NiFe (1.59 V) for the same current density. Rigorous stability assessments, including multi-step chronopotentiometry and continuous 100-h operation test (Figs. 3h and i), confirm exceptional operational stability with negligible activity decay. Quantitative Faradaic efficiency analysis was conducted *via* gasometric measurements at an industrially relevant current density of 200 mA/cm^2 (Figs. 3j and k). The near-perfect alignment between experimentally collected H_2/O_2 volumes and theoretically predicted values (Fig. 3l) reveals nearly 100 % Faradaic efficiency, confirming charge-transfer exclusivity toward water splitting [40,41]. The compatibility of the system with renewable power inputs (wind/solar/battery-driven operation) is demonstrated by continuous bubble evolution at electrodes under practical operating conditions (Fig. S8 in Supporting information). Crucially, the Ru/WP-MoP catalyst achieves unprecedented performance metrics in fully aqueous environments, surpassing not only the RuO_2||NiFe benchmark but also most cutting-edge catalysts reported for alkaline electrolytes.

The excellent OWS activity of the Ru/WP-MoP-based electrolyzer originates from its superior cathode HER activity, thus we further explored the intrinsic HER mechanism. Hydrogen binding energy (HBE) tests were conducted for both Ru/WP-MoP and the benchmark catalyst Ru/C [42]. Specifically, the hydrogen underpotential deposition (H_{upd}) peak of Ru/WP-MoP emerges at 0.180 V, in contrast to 0.203 V for Ru/C, directly demonstrating a weaker hydrogen adsorption strength on Ru/WP-MoP to boost the reaction kinetics (Fig. 4a) [43]. To reveal the catalytic mechanism of Ru/WP-MoP in alkaline media, LSV measurements were performed in 1 mol/L KOH/H_2O and 1 mol/L KOH/D_2O electrolytes. The voltage-dependent kinetic isotope effect (KIE = j_H/j_D) ranges from 2.4 to 2.8 within the potential window of -0.30∼-0.42 V (Fig. 4b). KIE values consistently exceeding 1.5 across all measured potentials confirm that hydrogen bond cleavage is involved in the rate-determining step [39,44,45]. Nyquist plots were employed to further investigate the hydrogen adsorption behavior. The hydrogen adsorption resistance (R_2) gradually decreases with increasing applied overpotential, indicating that more edge active sites are exposed, thereby accelerating charge transfer during the HER (Fig. 4c). *tert*-Butanol (TBA), a hydrogen radical quencher, was used to evaluate hydrogen adsorption strength [46]. The introduction of 1 mol/L TBA into

the KOH electrolyte causes a significant decline in the HER performance of both Ru/WP-MoP and WP-MoP (Fig. 4d). As shown in Fig. 4e, at 50 mA/cm^2, the activity of Ru/WP-MoP decays by 66.8 %. Notably, even at 100 mA/cm^2, the catalytic activity decay for Ru/WP-MoP is still superior to WP-MoP. The above results indicate that Ru/WP-MoP has a weaker hydrogen adsorption capacity, a characteristic beneficial to H_2 desorption and spillover over the catalyst surface [47,48]. Arrhenius analysis of temperature-dependent kinetics ultimately reveals superior catalytic efficiency of Ru/WP-MoP through remarkably low activation energies (9.7-10.7 kJ/mol *vs*. 12.5-15.3 kJ/mol for WP-MoP), demonstrating the cooperative effect of Ru incorporation and P vacancy engineering in reducing the HER energy barrier (Fig. 4f) [49].

After the HER durability testing, XRD results further verify that the phases of WP, MoP and Ru are still retained (Fig. S9a in Supporting information). Fig. S9b (Supporting information) shows the XRD patterns of Ru/WP-MoP before and after the HER test. The absence of any significant shift or disappearance in the characteristic peaks of the WP, MoP, and Ru phases indicates the excellent phase stability of the material during the HER process. Meanwhile, the SEM image shows complete retention of the coral-like 3D hierarchical porous architecture and overall electrode morphology after the reaction, with no structural collapse or detachment of active material, indicating excellent mechanical robustness (Fig. S9c in Supporting information). Moreover, the TEM result further corroborates the structural integrity at the nanoscale, as the coral-like nanoarchitecture remains intact after the durability test (Fig. S9d in Supporting information). Therefore, post-stability-test characterization data consistently demonstrates that the material retains outstanding structural and morphological stability.

We successfully engineered Ru-loaded tungsten-molybdenum bimetallic phosphide (Ru/WP-MoP) electrocatalysts through an ultrafast microwave-assisted *quasi*-solid-state synthesis strategy. The Ru/WP-MoP has exceptional HER performance, delivering 10 mA/cm^2 at 40 and 42 mV overpotentials to achieve in alkaline freshwater and simulated seawater electrolytes, respectively. The atomic dispersion of Ru sites within a coral-like hierarchical porous architecture of WP-MoP creates abundant accessible active sites, enabling nearly 100 % Faradaic efficiency during alkaline overall water splitting. Besides, the bimetallic W-Mo sites in WP-MoP induce strong EMSI with Ru, optimizing the d-band center of Ru, reducing its hydrogen binding energy. Ru reciprocally triggers P vacancy formation in WP-MoP, enhancing interfacial electron transfer. This innovative synthetic methodology establishes a versatile platform for defect-controlled fabrication of transition metal phosphides, while the demonstrated catalytic superiority under practical operating conditions provides crucial insights for advancing scalable green hydrogen technologies.

CRediT authorship contribution statement

Xueying Luan: Writing – original draft, Validation, Software, Methodology, Investigation, Formal analysis, Data curation. **Huilin Zhao:** Writing – review & editing, Validation, Supervision, Methodology, Data curation. **Yuhao Li:** Supervision. **Yusen Chen:** Validation, Supervision. **Hongdong Li:** Visualization. **Jun Xing:** Supervision, Conceptualization. **Yingxia Zong:** Validation, Supervision. **Weiping Xiao:** Validation, Supervision. **Guangying Fu:** Validation, Supervision. **Jinsong Wang:** Validation, Supervision. **Lei Wang:** Resources, Investigation, Formal analysis. **Zexing Wu:** Resources, Investigation, Formal analysis.

Declaration of competing interest

The authors declare that they have no known competing financial interests or personal relationships that could have appeared to influence the work reported in this paper.

Acknowledgments

The authors thank funding support from the National Natural Science Foundation of China (No. 52371227), Taishan Scholar Young Talent Program (No. tsqn202408200), Shandong Province "Double-Hundred Talent Plan" (No. WST2020003), the Natural Science Foundation of Shandong Province of China (No. ZR2021QE081).

Supplementary materials

Supplementary material associated with this article can be found, in the online version, at doi:10.1016/j.cclet.2026.112607.

References

[1] C.H. Li, C.Z. Yuan, X. Huang, et al., eScience 5 (2025) 100307.
[2] Z. Hu, H. Wu, X. Yong, et al., eScience 5 (2025) 100403.
[3] G. Liu, Y. Xu, T. Yang, L. Jiang, Nano Mater. Sci. 5 (2023) 101–116.
[4] J. Zhou, Y. Xie, L. Yang, et al., Inorg. Chem. Front. 10 (2023) 2842–2859.
[5] H. Zhao, M. Liu, X. Du, X. Zhang, Inorg. Chem. Front. 12 (2025) 2103–2112.
[6] L. Wang, X. Han, B. Xiong, et al., Chin. Chem. Lett. 36 (2025) 111437.
[7] M. Huo, Y. Liang, K. Qin, et al., Green Carbon 2 (2024) 403–404.
[8] Z. Song, N. Zhang, J. Yu, et al., Chin. Chem. Lett. 37 (2026) 111804.
[9] W. Song, J. Wu, J. Li, et al., Green Carbon 2 (2024) 393–400.
[10] A. Munir, J.Abdul Nasir, T.u. Haq, et al., Coord. Chem. Rev. 521 (2024) 216112.
[11] X. Zhou, T. Yang, T. Li, et al., Nano Res. Energy 2 (2023) e9120086.
[12] J. Mei, R. Guo, J. Zhao, et al., Appl. Catal. B: Environ. 383 (2026) 126089.
[13] X. Wang, Z. Zhang, H. Zhang, et al., Adv. Funct. Mater. 36 (2026) e14137.
[14] D. Liu, G. Xu, H. Yang, H. Wang, B.Y. Xia, Adv. Funct. Mater. 33 (2023) 2208358.
[15] P. Kuang, Y. Wang, B. Zhu, et al., Adv. Mater. 33 (2021) 2008599.
[16] Y. Feng, Y. Xie, Y. Yu, et al., Angew. Chem. Int. Ed. 64 (2025) e202413417.
[17] Y. Shi, Z.R. Ma, Y.Y. Xiao, et al., Nat. Commun. 12 (2021) 3021.
[18] J. Huang, Y. Jiang, T. An, M. Cao, J. Mater. Chem. A 8 (2020) 25465–25498.
[19] S.S. Lu, L.M. Zhang, Y.W. Dong, et al., J. Mater. Chem. A 7 (2019) 16859–16866.
[20] W. Du, Y. Shi, W. Zhou, Y. Yu, B. Zhang, Angew. Chem. Int. Ed. 60 (2021) 7051–7055.
[21] W. Xia, M. Zuo, Y. Li, et al., Electrochim. Acta 470 (2023) 143266.
[22] Y. Yang, X. An, D. Wang, et al., New J. Chem. 47 (2023) 19832–19837.
[23] X. Wang, H. Chen, B. Liu, et al., J. Power Sources 585 (2023) 233659.
[24] Z. Duan, M. Zhang, L. Cui, et al., J. Mater. Chem. A 10 (2022) 14435–14440.
[25] W. Chen, M. Hu, J. Zong, et al., Adv. Mater. 33 (2021) 2004930.
[26] H. Cheng, H. Liu, C. Huang, et al., Sep. Purif. Technol. 330 (2024) 125311.
[27] X. Qin, P. Ke, A. Wang, K.H. Kim, Surf. Coat. Technol. 228 (2013) 275–281.
[28] Z. Tang, X. Deng, Y. Zhang, et al., Sens. Actuator. B 297 (2019) 126730.
[29] C. Li, Y. Du, D. Wang, et al., Adv. Funct. Mater. 27 (2017) 1604328.
[30] C.Y. Son, I.H. Kwak, Y.R. Lim, J. Park, Chem. Commun. 52 (2016) 2819–2822.
[31] H. Chen, X. Zhang, S. Geng, S. Song, Y. Wang, Small Methods 6 (2022) 2200636.
[32] C. Wang, K. Liu, Y. Jin, S. Huang, J. Chun-Ho Lam, ChemSusChem 16 (2023) e202300222.
[33] K. Wang, X. Liu, Q. Yu, et al., Small 20 (2023) 2308613.
[34] Y. Hong, Y. Fu, J. Xiao, et al., J. Colloid Interface Sci. 699 (2025) 138117.
[35] H. Huang, K. Liu, F. Yang, et al., Angew. Chem. Int. Ed. 62 (2023) e202315752.
[36] K. Wang, X. Liu, Q. Yu, et al., Small 20 (2024) 2308613.
[37] Q. He, Y. Zhou, L. Mou, et al., Energy Environ. Sci. 18 (2025) 1984–1991.
[38] P. Su, W. Pei, X. Wang, et al., Angew. Chem. Int. Ed. 60 (2021) 16044–16050.
[39] X. Liu, X. Wang, K. Li, et al., Angew. Chem. Int. Ed. 63 (2024) e202316319.
[40] C. Zhao, J. Wang, Y. Gao, et al., Adv. Funct. Mater. 34 (2024) 2307917.
[41] Z. Niu, Z. Lu, Z. Qiao, et al., Adv. Mater. 36 (2024) 2310690.
[42] F. Lin, H. Luo, L. Li, et al., Nat. Synth. 4 (2025) 399–409.
[43] Z. Li, L. An, M. Song, et al., Chin. Chem. Lett. 34 (2023) 107622.
[44] P. Yan, T. Yang, M. Lin, et al., Adv. Funct. Mater. 33 (2023) 2301343.
[45] Z. Luo, Y. Guo, Y. Qian, et al., Adv. Funct. Mater. 34 (2024) 2405881.
[46] Y. Zhang, C. Ma, X. Zhu, et al., Adv. Energy Mater. 13 (2023) 2301492.
[47] Y. Zhang, C. Ma, X. Zhu, et al., Adv. Energy Mater. 13 (2023) 2301492.
[48] C. Zhang, H. Song, Z. Wang, et al., Small 20 (2024) 2311667.
[49] H. Wang, W. Cao, H. Sun, et al., Angew. Chem. Int. Ed. 65 (2026) e19688.